Time-resolved electrostatic force microscopy of polymer solar cells

DAVID C. COFFEY[1] AND DAVID S. GINGER[2]*

[1]Department of Physics, University of Washington, Seattle, Washington 98195-1560, USA
[2]Department of Chemistry, University of Washington, Seattle, Washington 98195-1700, USA
*e-mail: ginger@chem.washington.edu

Published online: 13 August 2006; doi:10.1038/nmat1712

Blends of conjugated polymers with fullerenes, polymers, or nanocrystals make promising materials for low-cost photovoltaic applications. Different processing conditions affect the efficiencies of these solar cells by creating a variety of nanostructured morphologies, however, the relationship between film structure and device efficiency is not fully understood. We introduce time-resolved electrostatic force microscopy (EFM) as a means to measure photoexcited charge in polymer films with a resolution of 100 nm and 100 μs. These EFM measurements correlate well with the external quantum efficiencies measured for a series of polymer photodiodes, providing a direct link between local morphology, local optoelectronic properties and device performance. The data show that the domain centres account for the majority of the photoinduced charge collected in polyfluorene blend devices. These results underscore the importance of controlling not only the length scale of phase separation, but also the composition of the domains when optimizing nanostructured solar cells.

In the pressing search for alternative energy sources, nanostructured organic solar cells are increasingly put forward as potential low-cost alternatives to conventional photovoltaics[1,2]. In a typical organic solar cell, light absorption creates strongly bound excitons that must be dissociated into free charges at a donor/acceptor interface[2–4]. The need for exciton dissociation complicates the design and fabrication of efficient organic solar cells because the light absorption depth is roughly ten times larger than the exciton diffusion range. Blended films with nanostructured donor/acceptor interfaces can provide a large internal surface area to support charge generation in optically thick films[2–6]. However, the complicated morphologies that arise in such blended films can lead to dramatic performance variations, as is readily observed when preparing films under different processing conditions[2,3,6–15].

Despite its importance, the exact correlation between film morphology and performance is still unclear. For instance, annealing polymer/fullerene blends can double their performance, but the mechanism is still under investigation[3,7–10]. Even in widely studied systems such as meso-phase-separated polyfluorene blends, different studies report that the bulk of the photocurrent arises alternatively from photogeneration at domain interfaces[11] or in the interior of the domains[16]. To address these and related issues, an imaging technique capable of mapping the photophysical properties of organic semiconductors with sub-100 nm resolution has become a highly sought experimental goal[16–25].

Herein, we report a scanning-probe technique for measuring photoexcited charge creation in organic thin films with better than 100 nm spatial resolution and 100 μs temporal resolution. We apply this technique to a model conjugated polymer blend to map charge generation as a function of local morphology and, contrary to our expectations, see that the majority of charge originates away from visible interfaces.

Previous efforts to image photophysical phenomena in polymer blends with high spatial resolution fall into two main classes: near-field scanning optical microscopy (NSOM) and scanning Kelvin probe microscopy (SKPM). Several groups have applied NSOM to characterize conjugated polymers[17–20] or have used an NSOM tip to photoexcite a device while measuring photocurrent[16,21–23]. Aside from the technical challenges associated with sub-100 nm

NSOM imaging, fluorescence and fluorescence quenching are indirect measures of charge generation, and their significance for photovoltaics is complicated because a large fraction of 'quenched' excitons result in geminate pairs which can recombine non-radiatively without contributing to the photocurrent[26,27]. In addition, NSOM-photocurrent and most NSOM-fluorescence experiments must use excitation intensities $\sim 10^3$ times higher than those found in an operating solar cell.

Electrostatic force microscopy (EFM) and SKPM have been instrumental in detailing charge injection[28,29], transport[29,30] and trapping[31,32] processes in organic transistors. Recently, several groups have applied SKPM to make surface potential maps of organic semiconductor blends under photoexcitation[24,25]. However, the relationship between static SKPM photovoltage images and the dynamic processes of charge generation and transport is unclear, and time resolutions sufficient to study photoinduced charging have not been reported. To address this problem, we use EFM to measure photogenerated carrier accumulation and surface potentials in a time-resolved fashion, and show that the measured EFM charge accumulation rates correlate with the external quantum efficiencies (EQEs) measured for completed devices.

We have chosen poly-(9,9′-dioctylfluorene-*co*-benzothiadiazole) (F8BT)/poly-(9,9′-dioctylfluorene-*co*-bis-*N*,*N*′-(4-butylphenyl)-bis-*N*,*N*′-phenyl-1,4-phenylenediamine (PFB) blends for our initial studies because this is a model system for studying the effects of film morphology on photovoltaic performance[11–13,24,33–36]. Nevertheless, the underlying mechanisms are not resolved. By correlating atomic force microscopy (AFM) topography with device performance, Snaith *et al.* concluded that the photocurrent was proportional to the interfacial area of the visible domain boundaries[11], whereas McNeill *et al.* used NSOM photocurrent data to conclude that more photocurrent may be collected inside the domains than at the boundaries[16].

In a steady-state EFM experiment, the tip is driven at its resonant frequency while hovering 5–100 nm above a surface, and the shift in the cantilever drive frequency required to keep the tip on resonance is measured as a voltage is applied between the tip and the sample[32,37]. The expected shift in resonance frequency of the cantilever, Δf, due to tip–sample electrostatic forces can be approximated by:

$$\Delta f \propto \frac{\partial^2 C}{\partial z^2}\left(V_{\mathrm{tip}} - V_{\mathrm{surface}}\right)^2. \qquad (1)$$

Here C is the capacitance between the tip and sample, z is the tip height above the sample, V_{tip} is the voltage applied to the tip and V_{surface} is the local surface potential. Figure 1 shows the results of such a steady-state EFM experiment on an F8BT/PFB blend film both in the dark and under constant illumination (molecular weights F8BT = 38 kg mol^{-1}, PFB = 22 kg mol^{-1}). The data in Fig. 1b are well described by equation (1), and demonstrate that illumination changes both the local surface potential and the tip–sample capacitance gradient. The change in capacitive gradient can be understood as follows: at non-zero tip voltages the photogenerated charges are drawn to the film surface beneath the tip by the electric field, increasing the tip–sample capacitive gradient (Fig. 1b, inset). After the tip–sample capacitor is fully charged (that is, there is enough accumulated space charge to cancel the internal field), net charge motion ceases, and local charge recombination will balance charge separation[27,33]. In this picture, the total frequency shift (total charge build-up) depends primarily on the applied voltage and not the light intensity over the range studied (because $|V_{\mathrm{tip}}| \gg |V_{\mathrm{surface}}|$ and V_{surface} depends only logarithmically on intensity[24,33,35,38]). We attribute the hysteresis under negative tip voltages in the dark to hole injection through

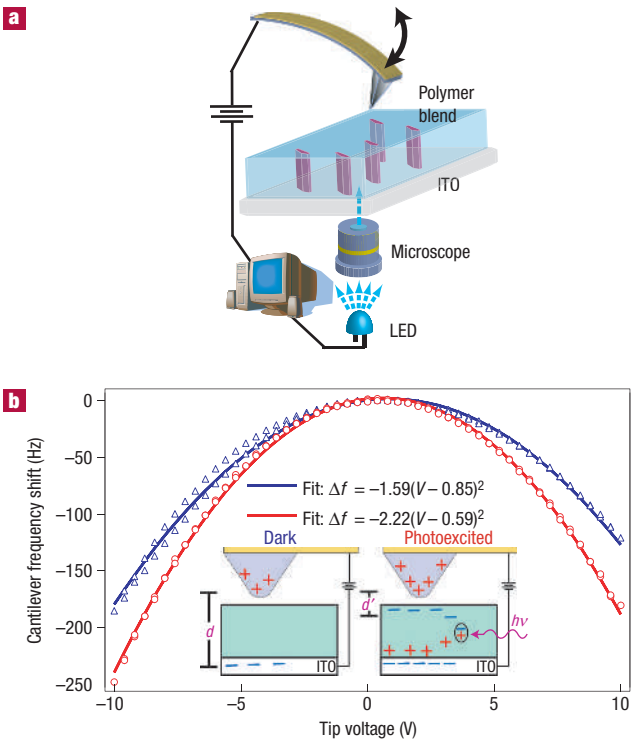

Figure 1 Measuring photoexcited charge with an AFM. a, Schematic diagram of a polymer blend illuminated with a pulsed LED through a transparent ITO electrode. Charge accumulation in the film is measured with a biased electrostatic force microscope tip using frequency-shift feedback. **b**, Cantilever frequency shift versus tip bias for an F8BT/PFB, 50:50, blend film in the dark (blue triangles) and under illumination (red circles), showing the expected parabolic dependence on frequency shift with bias, as well as a 260 mV decrease in surface potential (parabola offset) and an increase in tip–sample force gradient (parabola curvature) that accompany photocarrier generation. The solid lines are parabolic fits with the fitting equations given in the legend. Inset: Scheme showing how photoexcited charge changes the effective distance between capacitor plates (d to d') and thus increases the capacitive gradient measured by EFM.

the indium tin oxide (ITO, a transparent, conductive metal oxide) contact (see the Supplementary Information). All experiments were carried out in dry N_2 to prevent photooxidation.

Figure 2a shows the time evolution of the EFM frequency shift at +10 V tip bias during photoexcitation with 405 nm light. This wavelength was chosen to excite PFB and F8BT equally (Fig. 2b). After the light is turned on, the EFM signal follows a monotonic decay to a new equilibrium frequency value as charge generated by exciton dissociation fills the potential well created by the tip. The experimental charging curves are nearly single exponential with timescales that depend on film composition and are in the $\sim$0.5 ms range at $\sim$1 sun intensities for the 50:50 blends spin coated from xylenes. We do not suggest this characteristic timescale is associated with the time required for exciton dissociation across the donor/acceptor interface (which should be much faster[26,39]). Instead, we associate this timescale with the time constant of the self-limiting charging of the tip–sample capacitor, where the rate limiting step is the absorption of a sufficient number of photons (and their subsequent position-dependent dissociation and recombination rates) in the area underneath the tip to generate the charge required to fill the capacitor. A complete quantitative model would need to account for the full 3D field and charge

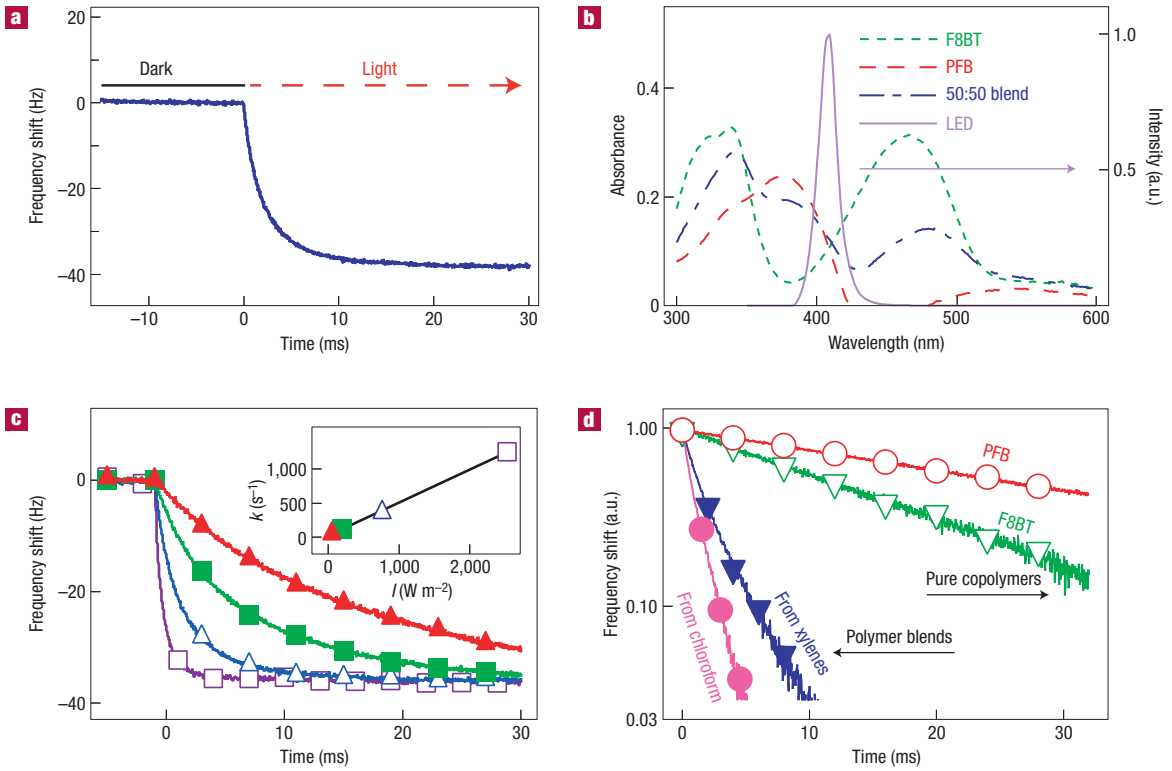

Figure 2 Time-resolving charge creation. a, Cantilever frequency shift versus time for a 50:50 film of F8BT/PFB after the light is turned on. **b**, The LED intensity spectrum (peak emittance near 405 nm) overlaid with the absorption spectra of three polymer films (as indicated in the legend) spin cast onto ITO. **c**, Normalized charge build-up versus time in the same film measured at four light intensities (50 W m^{-2}: filled triangles, 195 W m^{-2}: filled squares, 760 W m^{-2}: open triangles, 2,500 W m^{-2}: open squares), showing (inset) the linear dependence of charging rate on light intensity (black line: linear fit). **d**, Charge build-up versus time at 760 W m^{-2} plotted on a logarithmic scale as measured in four polymer films: pure PFB, pure F8BT, and 50:50 blends of F8BT/PFB spin cast from chloroform and xylenes, showing the increased rate measured in blend films.

profile surrounding the tip[37], while also accounting for any field dependence of the dissociation and recombination rates[27,40,41] of the geminate electron–hole pairs. Nevertheless, the picture of self-limiting charging of the tip–sample capacitor with a rate dependent on the intensity and local quantum efficiency is qualitatively consistent with the experimental data presented below. Consistent with this interpretation, Fig. 2c shows that the rate of charge accumulation scales linearly with light intensity. Furthermore, for donor/acceptor blends (but not for pure polymers) the charging rate is only weakly dependent on the tip bias, indicating that more excitons are dissociated by the donor/acceptor interfaces than by the applied field (see the Supplementary Information). The final magnitude of the frequency-shift value is independent of light intensity (and instead depends on the capacitor parameters of tip voltage and polymer film thickness, see the Supplementary Information). In addition, Fig. 2d shows that local photoinduced charging rates are an order of magnitude faster for a PFB/F8BT donor/acceptor blend than they are for either pure copolymer. Figure 2d also shows that, on average, donor/acceptor blend films cast from chloroform accumulate photoinduced charge faster than blend films cast from xylenes. Although each of these results is consistent with the device performance and EQEs of F8BT/PFB blends reported by others[11,12], it is important to note that the data are collected locally with the scanning-probe tip.

Significantly, we can use such data to create maps of local photoinduced charging rates with high spatial resolution. To do so, we acquire EFM charging curves like those in Fig. 2a,c,d in point-by-point fashion above the sample and then plot the value of the fitted exponential rate constant at each point. The surface topography together with a charging rate map is plotted in Fig. 3a,b for a 50:50 wt% blend of F8BT/PFB spin coated from xylenes. The film topography shows the classic submicron morphology typical of F8BT/PFB films processed from xylenes[11–13,34], and we assign the regions of lower topography to PFB-rich domains through far-field fluorescence microscopy on a series of blend films.

The charge generation map in Fig. 3b shows that the charging rate varies by more than a factor of two across the surface of the film, with the smallest features corresponding to a spatial resolution better than 100 nm. Figure 3b also reveals features not visible in the topography, suggesting the presence of submerged polymer domains as have been previously observed by NSOM[19]. Although the smallest features in our images match typical EFM resolutions of ~50–100 nm, it is important when interpreting both the temporal and spatial resolution of our measurement to consider the possibility that the EFM signal might incorporate lateral charge diffusion from sites very far from the tip. Although this hypothesis cannot be excluded, we find it less likely for two reasons. First, finite element calculations suggest that 50% of the field is concentrated within 40 nm of the tip[37]. Second, and more importantly, by experimentally measuring charging rates as the cantilever approaches a sharp step edge in the polymer, we have determined that in our experiments ~80% of the collected charge originates within 90 nm of the tip (see the Supplementary Information). On the basis of this resolution, the final frequency shift of 50 Hz observed in Fig. 2c corresponds to an estimated $\sim 3 \times 10^{-17}$ C of charge collected from an area of $\sim\pi(90\,\text{nm})^2$.

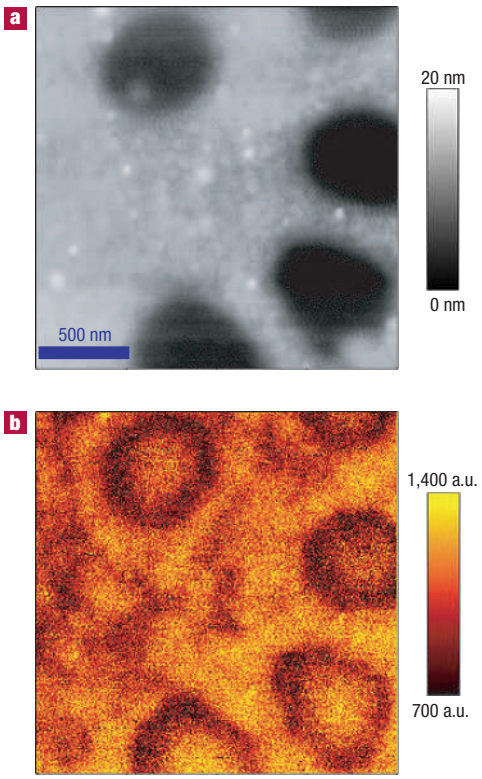

Figure 3 Charging rate image of a polymer blend film. a, AFM height image of a 50:50 film of F8BT/PFB spin coated from xylenes. The recessed domains are enriched in PFB (film thickness: 90 nm). **b**, EFM photoinduced charging rate map generated by plotting the inverse exponential time constant for photoinduced charging at each point in **a**. The dark rings indicate regions of slower charging.

The most striking feature of Fig. 3a,b is that charge generation seems slowest at the interfaces between polymer domains. Each dark ring corresponds to a region where charge accumulates under the tip ~30–50% slower than in the surrounding regions. This result contradicts our initial assumption that the donor/acceptor domain boundaries should always correspond to the regions of fastest photoinduced charging and serves to emphasize the important contribution microscopic imaging can make towards the understanding of organic solar cells. We have conducted control experiments on both blended and unblended polymer samples (see the Supplementary Information) to check for topographic and scanning artefacts as the source of the rings, but we do not observe comparable changes in charging rate for either raised topographic features or lateral drops over three times as severe as those present in the studied blends. In addition, the contrast in rate features disappears at negative tip bias when rapid hole injection from the ITO contact competes with photocarrier generation. We discuss possible causes for the slow rings after comparing our EFM images with bulk device quantum efficiency measurements below.

If local scanned probe measurements are to provide insight into device operation, they must correlate with device performance. Figure 4 compares the spatially averaged (over a $3 \times 3\,\mu m^2$ image) charging rate measured by EFM with the short circuit EQE for a series of photodiodes ($\sim 4\,mm^2$ in area) prepared from blends of varying F8BT/PFB ratios.

Figure 4a is a key figure in this manuscript, and shows that the EFM charging-rate values and device EQEs are well correlated, providing strong validation for the use of our method. We hypothesize that the agreement is particularly good because for positive tip bias the EFM experiment measures how easily electrons are photogenerated and subsequently accumulated at the top film surface, mimicking current generation in a full ITO|F8BT/PFB|Al device illuminated through the ITO where electron collection at the top cathode is thought to be the rate-limiting process[35]. Figure 4a also shows a complicated relationship between the EQE values and the blend composition (see also Supplementary Information). All blends are significantly more efficient than the pure polymers, and the maximum EQE and charging rate both occur in blends with more F8BT than PFB. These broad trends are qualitatively consistent with the extensive studies by Friend and co-workers on this system[11,12,35,36], however, the data in Fig. 4a show some noteworthy differences.

Although the maximum EQE in Fig. 4a occurs at an F8BT/PFB ratio of 65:35, similar to that reported by Snaith *et al.*[11], we do not observe the same correlation between interfacial area and device performance. Indeed, Fig. 4bII,III show the slowest photoinduced charging rates near the microscale domain interfaces. Consistent with these EFM images, the film with the highest EQE also shows the fewest microscale interfaces (Fig. 4bIV). One possible explanation for this difference between our results and those of Snaith *et al.* lies in materials and preparation differences: we spin coated our polymers directly onto ITO as opposed to a polymer hole-transport layer, which could lead to differences in fine mixing as well as vertical phase separation.

More importantly, however, our data show that the increased performance observed for the films shown in Fig. 4bI–IV cannot be attributed solely to changes at visible domain interfaces. In comparison, the background charging rate within the large domains increases by a factor of 30 as the F8BT fraction is varied from 0 to 65%. This observation, and the correlation of the average charging rate with the device EQE, suggest that a significant fraction of the photocurrent may actually arise from charge generated and collected within the middle of the large domains, consistent with NSOM measurements[16,22]. Furthermore, whereas the most dramatic increase in charge generation occurs over the polymer ratios where the large circular PFB domains disappear (46%–52% F8BT in our films), the similarly abrupt ~40% increase in the background charging rate accounts for most of the observed average increase. Significantly, it seems that not only do the centres of the domains generate and collect much of the charge, but that their efficiency at doing so increases considerably as the F8BT concentration is increased. This effect could be due to unresolved changes in fine lateral phase separation or to changes in vertical[36] phase separation and suggests that carrier lifetimes and mobilities on the minority phases in each domain are important factors.

Finally, we discuss the rings of slow charging observed in Figs 3b and 4bII,III. This apparent reduction in charging rate at the domain interfaces could arise from several sources. First, low-molecular-weight species and chain ends tend to migrate to interfaces[42]. However, purifying the polymers by Soxhlet extraction had little effect on either the size or magnitude of the rings. Furthermore, blend ratios of 15:85 and 30:70 do show increased charging rates near domain interfaces. Second, although donor–acceptor interfaces lead to enhanced carrier generation, they also facilitate recombination[35,39], so the quantum yield of carriers that reach the surface near an interface may be diminished. Finally, the contrast could result from compositional gradients and variations in the degree of intermixing that can occur near polymer domain boundaries[43]. The film generates charge far from the apparent domain boundaries because the PFB-rich and F8BT-rich phases are not pure: the PFB-rich phase contains F8BT and *vice versa*. Thus, a reduction in charge generation could be explained if there was less PFB in the F8BT-rich domain very close to the interface in our

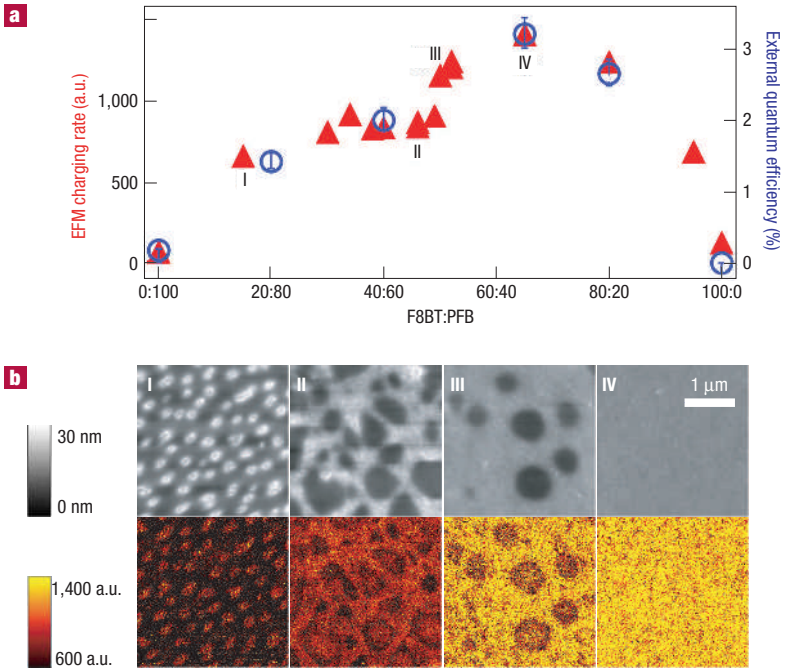

Figure 4 Correlating charging rate and EQE. a, Overlaying average EFM charging rate (red triangles) and device EQE (blue circles) for polymer films with varying F8BT/PFB ratios. The error bars in the EQE data were calculated by multiplying the measured EQE by the relative uncertainty in the measured active area for each diode. **b**, AFM topography (upper panels) and EFM charging rate (lower panels) images for the four ratios identified in **a**.

blends. This hypothesis is consistent with the increase in poly(9,9′-dioctylfluorene), (PFO), fluorescence at the domain boundaries in NSOM experiments in F8BT:PFO blends studied by Lidzey *et al.*[17]. A definitive resolution of this question will require high-resolution measurements of both local carrier recombination rates and film composition. Nevertheless, our results emphasize the importance of understanding the local compositional and optoelectronic properties of the film—not just the domain morphology—when making structure–function correlations in excitonic solar cells.

In conclusion, we have shown that spatial averages of the locally measured photoinduced charging rates are directly proportional to the EQEs of photodiodes prepared from F8BT/PFB blends. Having correlated local charging rates with the EQE of devices, we can identify the domains in complicated nanostructured films that give rise to the most photocurrent. In the F8BT/PFB blends studied we observe slower charging near the microscale domain boundaries and associate the bulk of the photocurrent with regions away from the visible domain interfaces. Thus, with regard to the question of whether the mesocale domain interfaces[11], or the domain centres[16] are responsible for the most photocurrent in these model blends, our data suggest it is the domain centres. These results indicate that the composition of the phase-separated domains can have a potentially stronger effect on device performance than the observable mesoscale film morphology, and that optimizing carrier transport and recombination rates within these domains by controlling domain composition could improve the performance of devices based on phase-separated donor/acceptor blends. Such results highlight the need for—and the reported method provides the means to obtain—more detailed information on local optoelectronic properties in organic semiconductor films. Although we have focused on photoinduced charging, recombination and trapping can also occur on micro- to milli-second timescales, and are accessible with minor modifications of the experiment. The importance of these issues is not limited to polymer blends, but is central to building a microscopic understanding of photovoltaic cells based on polymers, small molecules, and dye-sensitized metal oxides.

METHODS

DEVICE FABRICATION

ITO substrates, with a resistance of 20 ohms per square, were purchased (Thin Film Devices). These substrates were sonicated in acetone and then in isopropanol for 10 min each and then plasma cleaned for 5 min (Harrick Plasma cleaner, model PDC-32G) at medium power with air as the leakage gas.

All polymers were purchased (American Dye Source) and used as supplied except for the explicitly noted Soxhlet extraction experiment. Soxhlet extraction was carried out with acetone for 48 h and the insoluble fraction used in later experiments. The F8BT and PFB had molecular weights of 38 and 22 kg mol^{-1}, respectively, as indicated by the manufacturer. All polymers were dissolved in chloroform or xylenes at weight fractions of 20 mg ml^{-1}, filtered through a 0.45 μm polytetrafluoroethylene filter, and spin coated at 2,000 revolutions min^{-1}. The absorption spectra were taken on an Agilent 8453 spectrophotometer.

EXTERNAL QUANTUM EFFICIENCIES

External quantum efficiencies were measured in a home-built vacuum chamber at ~5 mtorr. Aluminium contacts, 60-nm thick, were thermally evaporated through a shadow mask. Samples were illuminated by a 75 W xenon lamp (Spectra Physics model 60100) filtered by a monochrometer (Acton Spectra Pro 2150i). Photocurrents were recorded by a Keithly 2400 source meter, and the EQE were determined by taking the ratio of the device photocurrent with that of a Si photodiode with known spectral response.

ATOMIC AND ELECTRIC FORCE MICROSCOPY MEASUREMENTS

Atomic and electric force microscopy measurements were carried out on an Asylum Research MFP-3D AFM mounted on a Nikon TE2000-U inverted optical microscope. Samples were placed in a sealed fluid cell and flushed with nitrogen beginning 5 min before any illumination. We used platinum-coated

cantilevers (Budget Sensors BS-ElectriTap300) with spring constants of ~40 N m^{-1}, quality factors of ~480 and resonant frequencies of ~300 kHz. The data in each figure was obtained with the same AFM tip. The MFP-3D controller was programmed to apply voltages to the AFM tip and to turn the light emitting diode (LED) on and off. The LED (LEDtronics; part L200CUV405-8D, 405 nm peak emittance) was focused through the back of the microscope and up a ×40 air objective. The field stop was set so that the area illuminated was ~200 μm in diameter. Neutral density filters were inserted between the LED and optical microscope as necessary to keep the charging rates ~1,000 Hz.

To measure photoinduced charging underneath the tip, specifically as in Fig. 2a, the tip is raised 15 nm above the surface and set at +10 V relative to the ITO. At time equals zero, the LED illuminates the surface for 30 ms. The light and voltage are turned off for another 32 ms to allow the charge to dissipate, before repeating this process 500 times and averaging the data. The time resolution is limited by the controller's frequency feedback loop and its response to noise, both environmental and thermo-mechanical[37]. Practically, ~100 μs resolution is relatively easy to achieve with stable gain settings in our laboratory (as seen by the cantilever's distinct response to two voltage pulses), and thus the nearly exponential behaviour is not instrument limited but indicates a self-limiting capacitive charging process associated with the collection of photogenerated carriers underneath the biased tip.

For charging rate images as in Fig. 3, this procedure is repeated at each pixel except without averaging and with shorter wait times. Each line of the sample is first scanned in normal intermittent contact mode. The tip oscillation is reduced to an amplitude ~15 nm and the entire cantilever lowered to place the bottom extension of the tip ~15 nm above the surface. The cantilever drive frequency is set in a frequency feedback loop to keep the cantilever on resonance (the feedback integral and proportional gains are chosen to give a response time ~100 μs). As the tip is retraced across the sample in this raised mode, the charge build-up is recorded at each point in the scan line. To achieve this for an F8BT/PFB blend, first, the voltage is turned on for 1 ms, during which time the cantilever stabilizes. Second, the LED is turned on for 5 ms and the charge/frequency shift build-up recorded (this data is later fitted, without averaging, to an exponential and the rate, magnitude and error recorded). Third, the voltage difference is returned to zero while the light is kept on for 2 ms, allowing the collected charge to dissipate. Finally, to further equilibrate the sample, the light is turned on for another 2 ms. This cycle is repeated at every point (~256) in a scan line.

Received 26 April 2006; accepted 17 July 2006; published 13 August 2006.

References

1. Nelson, J. Solar energy—Solar cells by self-assembly? *Science* **293,** 1059–1060 (2001).
2. Shaheen, S. E., Ginley, D. S. & Jabbour, G. E. Organic-based photovoltaics. toward lowm-cost power generation. *Mater. Res. Soc. Bull.* **30,** 10–19 (2005).
3. Hoppe, H. & Sariciftci, N. S. Organic solar cells: An overview. *Mater. Res. Soc. Bull.* **19,** 1924–1945 (2004).
4. Gregg, B. A. The photoconversion mechanism of excitonic solar cells. *Mater. Res. Soc. Bull.* **30,** 20–22 (2005).
5. Halls, J. J. M. *et al.* Efficient photodiodes from interpenetrating polymer networks. *Nature* **376,** 498–500 (1995).
6. Yu, G., Gao, J., Hummelen, J. C., Wudl, F. & Heeger, A. J. Polymer photovoltaic cells—enhanced efficiencies via a network of internal donor-acceptor heterojunctions. *Science* **270,** 1789–1791 (1995).
7. Chirvase, D., Parisi, J., Hummelen, J. C. & Dyakonov, V. Influence of nanomorphology on the photovoltaic action of polymer-fullerene composites. *Nanotechnology* **15,** 1317–1323 (2004).
8. Padinger, F., Rittberger, R. S. & Sariciftci, N. S. Effects of postproduction treatment on plastic solar cells. *Adv. Funct. Mater.* **13,** 85–88 (2003).
9. van Duren, J. K. J. *et al.* Relating the morphology of poly(p-phenylene vinylene)/methanofullerene blends to solar-cell performance. *Adv. Funct. Mater.* **14,** 425–434 (2004).
10. Kim, Y. *et al.* A strong regioregularity effect in self-organizing conjugated polymer films and high-efficiency polythiophene: fullerene solar cells. *Nature Mater.* **5,** 197–203 (2006).
11. Snaith, H. J., Arias, A. C., Morteani, A. C., Silva, C. & Friend, R. H. Charge generation kinetics and transport mechanisms in blended polyfluorene photovoltaic devices. *Nano Lett.* **2,** 1353–1357 (2002).
12. Arias, A. C. *et al.* Photovoltaic performance and morphology of polyfluorene blends: A combined microscopic and photovoltaic investigation. *Macromolecules* **34,** 6005–6013 (2001).
13. Moons, E. Conjugated polymer blends: linking film morphology to performance of light emitting diodes and photodiodes. *J. Phys. Condens. Matter* **14,** 12235–12260 (2002).
14. Coakley, K. M., Liu, Y. X., Goh, C. & McGehee, M. D. Ordered organic-inorganic bulk heterojunction photovoltaic cells. *Mater. Res. Bull.* **30,** 37–40 (2005).
15. Coffey, D. C. & Ginger, D. S. Patterning phase separation in polymer films with dip-pen nanolithography. *J. Am. Chem. Soc.* **127,** 4564–4565 (2005).
16. McNeill, C. R., Frohne, H., Holdsworth, J. L. & Dastoor, P. C. Near-field scanning photocurrent measurements of polyfluorene blend devices: Directly correlating morphology with current generation. *Nano Lett.* **4,** 2503–2507 (2004).
17. Chappell, J. *et al.* Correlating structure with fluorescence emission in phase-separated conjugated-polymer blends. *Nature Mater.* **2,** 616–621 (2003).
18. McNeill, J. D. & Barbara, P. F. NSOM investigation of carrier generation, recombination, and drift in a conjugated polymer. *J. Phys. Chem. B* **106,** 4632–4639 (2002).
19. Stevenson, R. *et al.* Fluorescence scanning near-field optical microscopy of polyfluorene composites. *J. Microsc.-Oxford* **202,** 433–438 (2001).
20. Cadby, A., Dean, R., Fox, A. M., Jones, R. A. L. & Lidzey, D. G. Mapping the fluorescence decay lifetime of a conjugated polymer in a phase-separated blend using a scanning near-field optical microscope. *Nano Lett.* **5,** 2232–2237 (2005).
21. DeAro, J. A., Moses, D. & Buratto, S. K. Near-field photoconductivity of stretch-oriented poly(para-phenylene vinylene). *Appl. Phys. Lett.* **75,** 3814–3816 (1999).
22. Riehn, R. *et al.* Local probing of photocurrent and photoluminescence in a phase-separated conjugated-polymer blend by means of near-field excitation. *Adv. Funct. Mater.* **16,** 469–476 (2006).
23. McNeill, C. R. & Dastoor, P. C. Photocurrent pattern formation in polymer/methanofullerene blends imaged by near-field scanning photocurrent microscopy. *J. Appl. Phys.* **99,** 033502 (2006).
24. Chiesa, M. *et al.* Correlation between surface photovoltage and blend morphology in polyfluorene-based photodiodes. *Nano Lett.* **5,** 559–563 (2005).
25. Hoppe, H. *et al.* Kelvin probe force microscopy study on conjugated polymer/fullerene bulk heterojunction organic solar cells. *Nano Lett.* **5,** 269–274 (2005).
26. Russell, D. M. *et al.* Efficient light harvesting in a photovoltaic diode composed of a semiconductor conjugated copolymer blend. *Appl. Phys. Lett.* **80,** 2204–2206 (2002).
27. Koster, L. J. A., Smits, E. C. P., Mihailetchi, V. D. & Blom, P. W. M. Device model for the operation of polymer/fullerene bulk heterojunction solar cells. *Phys. Rev. B* **72,** 085205 (2005).
28. Burgi, L., Richards, T. J., Friend, R. H. & Sirringhaus, H. Close look at charge carrier injection in polymer field-effect transistors. *J. Appl. Phys.* **94,** 6129–6137 (2003).
29. Silveira, W. R. & Marohn, J. A. Microscopic view of charge injection in an organic semiconductor. *Phys. Rev. Lett.* **93,** 116104 (2004).
30. Burgi, L., Richards, T., Chiesa, M., Friend, R. H. & Sirringhaus, H. A microscopic view of charge transport in polymer transistors. *Synth. Met.* **146,** 297–309 (2004).
31. Palermo, V., Palma, M. & Samori, P. Electronic characterization of organic thin films by Kelvin probe force microscopy. *Adv. Mater.* **18,** 145–164 (2006).
32. Muller, E. M. & Marohn, J. A. Microscopic evidence for spatially inhomogeneous charge trapping in pentacene. *Adv. Mater.* **17,** 1410–1414 (2005).
33. Ramsdale, C. M. *et al.* The origin of the open-circuit voltage in polyfluorene-based photovoltaic devices. *J. Appl. Phys.* **92,** 4266–4270 (2002).
34. Ramsdale, C. M. *et al.* ESEM imaging of polyfluorene blend cross-sections for organic devices. *Physica E* **14,** 268–271 (2002).
35. Snaith, H. J., Greenham, N. C. & Friend, R. H. The origin of collected charge and open-circuit voltage in blended polyfluorene photovoltaic devices. *Adv. Mater.* **16,** 1640–1645 (2004).
36. Arias, A. C. *et al.* Vertically segregated polymer-blend photovoltaic thin-film structures through surface-mediated solution processing. *Appl. Phys. Lett.* **80,** 1695–1697 (2002).
37. Tevaarwerk, E., Keppel, D. G., Rugheimer, P., Lagally, M. G. & Eriksson, M. A. Quantitative analysis of electric force microscopy: The role of sample geometry. *Rev. Sci. Instrum.* **76,** 053707 (2005).
38. Koster, L. J. A., Mihailetchi, V. D., Ramaker, R. & Blom, P. W. M. Light intensity dependence of open-circuit voltage of polymer: fullerene solar cells. *Appl. Phys. Lett.* **86,** 123505 (2005).
39. Morteani, A. C., Friend, R. H. & Silva, C. Exciton trapping at heterojunctions in polymer blends. *J. Chem. Phys.* **122,** 244906 (2005).
40. Barker, J. A., Ramsdale, C. M. & Greenham, N. C. Modeling the current-voltage characteristics of bilayer polymer photovoltaic devices. *Phys. Rev. B* **67,** 075205 (2003).
41. Tanase, C., Meijer, E. J., Blom, P. W. M. & de Leeuw, D. M. Unification of the hole transport in polymeric field-effect transistors and light-emitting diodes. *Phys. Rev. Lett.* **91,** 216601 (2003).
42. Bucknall, D. G. Influence of interfaces on thin polymer film behaviour. *Prog. Mater. Sci.* **49,** 713–786 (2004).
43. McNeill, C. R. *et al.* Nanoscale quantitative chemical mapping of conjugated polymer blends. *Nano Lett.* **6,** 1202–1206 (2006).

Acknowledgements

We thank O. Reid and Y. Chen for their experimental assistance, Asylum Research for their continuing help, M. Chiesa and R. Shikler for their comments on the manuscript and H. Snaith for his comments and for valuable discussions. This material is based on work supported by the National Science Foundation (DMR 0449422) and the STC Program of the National Science Foundation (DMR 0120967).
Correspondence and requests for materials should be addressed to D.S.G.
Supplementary Information accompanies this paper on www.nature.com/naturematerials.

Competing financial interests

The authors declare that they have no competing financial interests.